



IGC Newsletter

IN THIS ISSUE

Technical Articles

- Spectroscopic Studies using Solid Para-Hydrogen Matrix
- Non-destructive Waste Assay Computed Tomography (NDWACT) System

Young Officer's Forum

- Comparison of Structural Reliability of Forged versus Welded Tri - Junction Joint in Dome Shaped Roof Slab of CBR

Young Researcher's Forum

- Effect of Impurities on Physicochemical Properties of Group III Nitride Nanowires

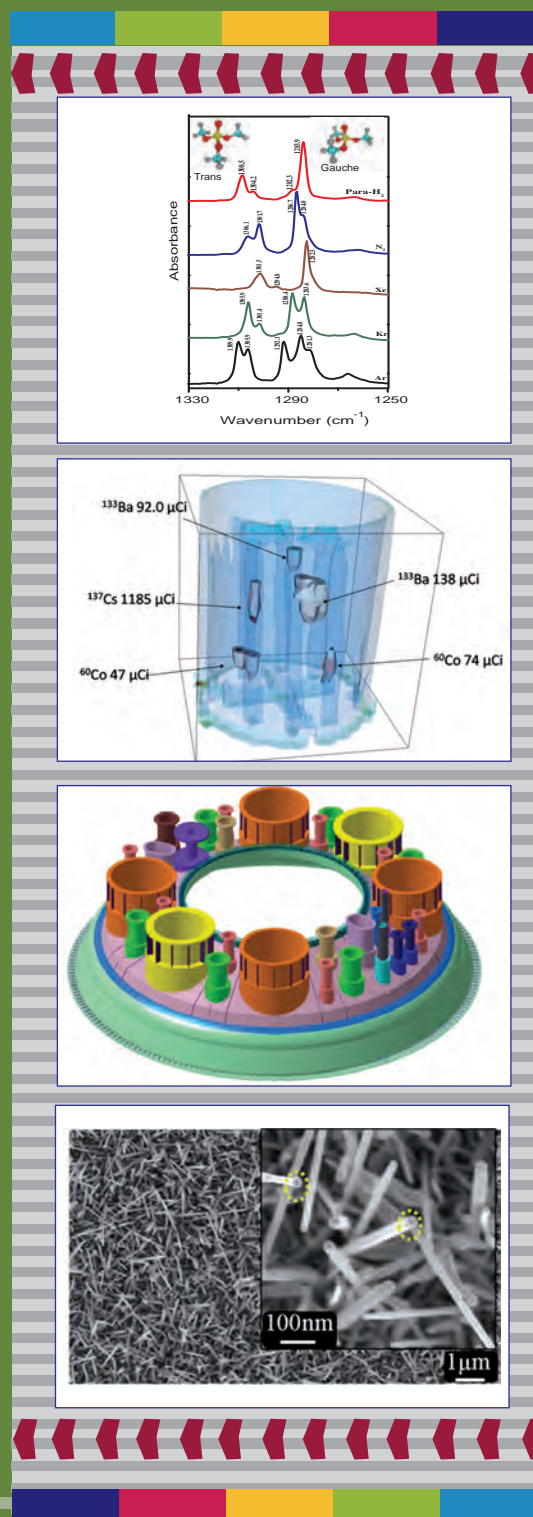
News & Events

- Graduation Function of the 10th Batch of Trainee Scientific Officers of BARC Training School at IGCAR
- BITS Practice School
- Summer Training in Physics & Chemistry (STIPAC-2016)
- Hindi Fortnight Celebration

Conference and Meeting Highlights

- 10th National Conference on Recent Advances in Information Technology
- A brief report on Hindi Scientific Seminar
- Quality Circle Annual Meet (QCAM)
- 8th CEA-DAE Steering Committee Meeting on JHR Collaboration

Awards & Honours



From the Editor

Dear Reader

It is my pleasant privilege to forward a copy of the latest issue of IGC Newsletter (Volume 110, October 2016 issue).

In the first technical article Dr. Sundararajan and colleagues have discussed the design, development and fabrication of p-H₂ converter and use of solid para-Hydrogen matrix for matrix isolation experiments of guest molecules at low temperature for the first time in our Country.

In the second technical article Shri R. Ramar and colleagues have shared their experience regarding the indigenous development and commissioning of a fully automated waste assay computed tomography system for the assay of waste materials.

This issue's young officer's forum features an article by Shri Vinoth on the comparison of structural reliability of forged and welded tri-junction joint in dome shaped roof slab of commercial fast breeder reactor.

Shri Avinash Patsha has studied the effect of impurities on Physicochemical Properties of Group III Nitride nanowires in young researcher's forum.

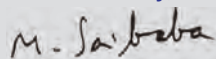
This Newsletter carries reports on the "Graduation Function of the 10th Batch of Trainee Scientific Officers of BARC Training School at IGCAR", "BITS Practice School", "Summer Training in Physics and Chemistry (STIPAC -2016)", "Hindi Fortnight Celebration", "10th National Conference on Recent Advances in Information Technology (READIT-2016)", "Hindi Scientific Seminar", "Quality Circle Annual Meet" and "8th CEA-DAE Steering Committee Meeting".

We are happy to share with you the awards, honours and distinctions earned by our colleagues.

We look forward to your comments, continued guidance and support.

With my best wishes and personal regards,

Yours sincerely,



(M. Sai Baba)

Chairman, Editorial Committee, IGC Newsletter

&

Director, Resources Management Group

Spectroscopic Studies using Solid Para-Hydrogen Matrix

High resolution spectroscopy of molecules in condensed phase becomes possible due to the advent of matrix isolation technique. In a matrix isolation experiment, the molecule of interest is mixed along with an inert gas (Ne/Ar/Kr/Xe/N₂) in a typical ratio of 1:1000 and deposited at low temperatures. Though the technique has been extensively used in the field of molecular spectroscopy to study the hydrogen-bonded interactions, conformations, radicals etc. The conventional matrix gases are not truly 'inert' and have limitations due to solute-matrix interaction and multiple trapping sites. In recent times, solid hydrogen has been identified as an alternate and promising matrix material in place of conventional matrix gases. The hydrogen molecule at room temperature exists in ortho and para forms in a ratio 3:1 and it is a real challenge to prepare pure p-H₂ gas from n-H₂. Due to small mass and large amplitude zero-point vibration with the reasonably high triple point of 13.8 K, para hydrogen (p-H₂) is being referred to as 'quantum crystal'. This is the first time the utility of p-H₂ gas is being demonstrated in our country and this article highlights the production of para-Hydrogen through enrichment of normal hydrogen gas and its use as matrix gas for matrix isolation experiment of guest molecules. The sharp line-width in solid p-H₂ in comparison to conventional matrices is a consequence of its exceptional spectroscopic properties. The p-H₂ crystal provides a homogeneous and interaction free environment for guest molecules embedded in it due to the spherical and symmetric (J=0 rotational wave function) nature unlike ortho-H₂ (o-H₂). The solid p-H₂ crystallizes in a pure hexagonal-closed packed (hcp) lattice, contrary to other inert and diatomic matrix gases, making the optical spectra simple and

sharp. The intrinsically restless nature of p-H₂ even at absolute zero temperatures owing to the large zero-point energy of the solid p-H₂ makes the multiple trapping sites and crystal defects around the guest molecules to be self-repaired. In addition, the large lattice constant of solid p-H₂ makes the interaction between the guest and the host molecules weak and as a result, the life time of the excited states of the guest molecules in solid p-H₂ becomes longer. These unique properties make the p-H₂ a promising matrix material to study the molecular properties of molecules at low temperatures, which can mimic the gas phase behavior. The insignificant or diminished cage effect is an attractive property of p-H₂ to study the photo-products including radicals under isolated conditions.

To make use of the p-H₂ properties mentioned above, pure p-H₂ gas is obtained from enrichment of normal hydrogen gas (n-H₂) (3: 1 ortho/para ratio; 75% will be in ortho form and 25% in para form). The enrichment can be achieved when n-H₂ gas is passed through a catalyst at low temperatures. We have designed, developed and fabricated an ortho-para (o/p) converter and incorporated it into a low temperature cryostat. The o/p converter consists of a copper bobbin onto which a copper tube filled with hydrated iron (III) oxide as catalyst was wrapped over and soldered to give good contact. The temperature of the bobbin/catalyst was maintained at 13.5 K and the flow rate of n-H₂ gas was adjusted through a fine dosing valve and passed onto the catalyst. The schematic of the p-H₂ converter is shown in Figure 1. It takes typically around 30 minutes for the conversion of n-H₂ to p-H₂. The converter is capable of producing p-H₂ gas of purity >99%. The o/p converter can be used to produce a wide range of p-H₂

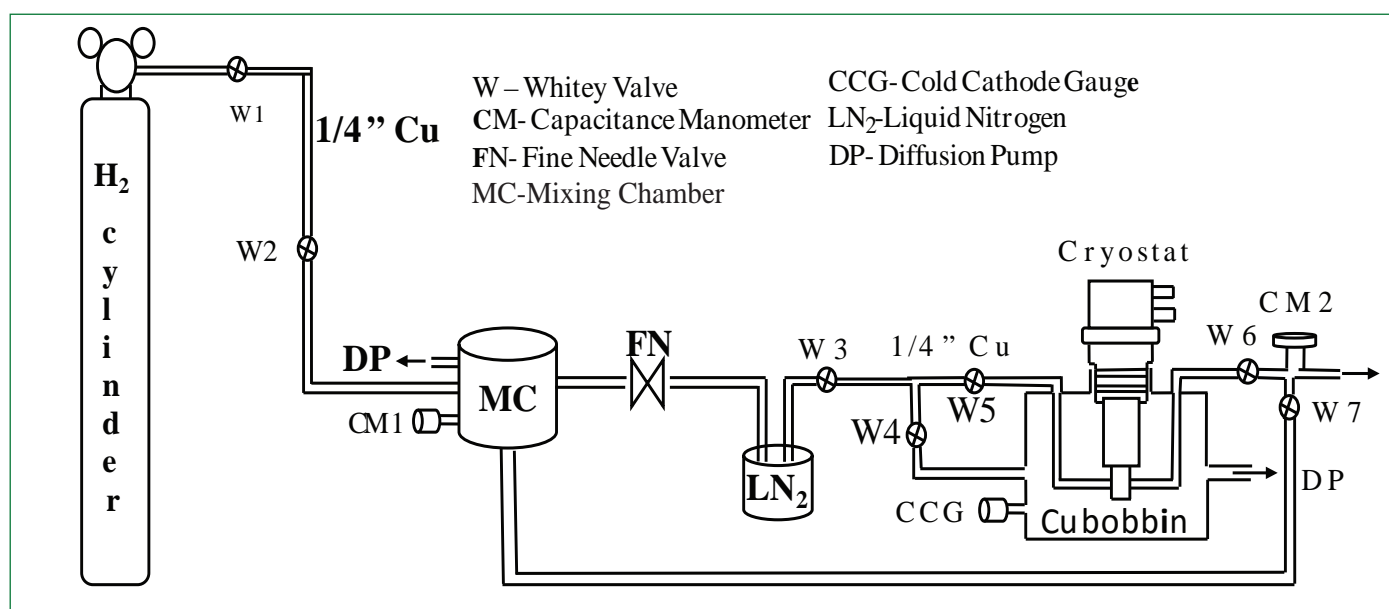


Figure 1: Schematic of the para-hydrogen set-up



Figure 2: Photographs showing the p-H₂ generation set-up

enrichments. p-H₂ generation and deposition set-ups are shown in Figures 2 and 3. The collected gas was analyzed using Raman and low temperature infrared spectroscopic studies. Figure 4 gives the typical infrared spectrum of p-H₂ solid recorded at different temperatures 13.5, 20 and 25 K. In the same Figure solid n-H₂ is also shown for comparison. It can be seen from the figure that as the temperature of the bobbin increases the Q₁(O) transition observed at

4152.8 cm⁻¹ increases, which gives the estimate of %o-H₂ impurity in p-H₂ matrix. The analysis of the infrared spectrum of p-H₂ clearly revealed that the percentage o-H₂ in p-H₂ matrix at different temperatures was found to be 0.7, 2.6, and 4.3 respectively.

The p-H₂ gas thus produced was collected in a bulb and mixed with trimethyl phosphate (TMP) to study its structural properties. The mixture was then deposited onto a KBr substrate kept at 2.5 K.



Figure 3: Photographs showing the p-H₂ (a) generation and (b) deposition set-up

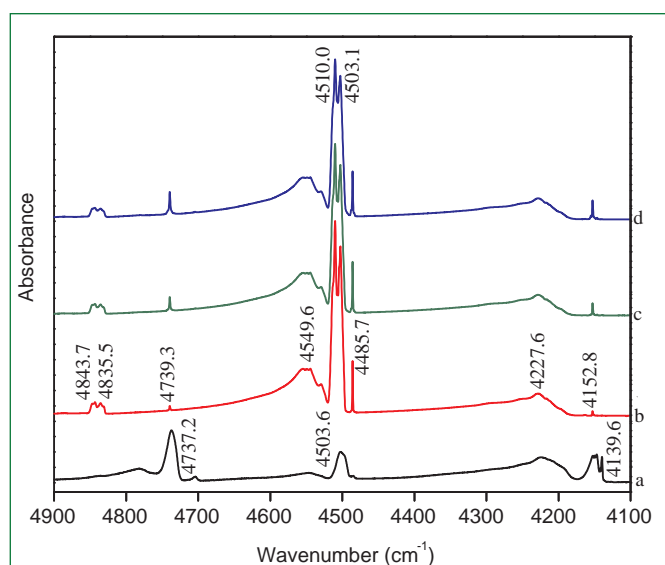


Figure 4: Infrared absorption spectra covering the region 4900-4100 cm⁻¹ (a) n-H₂; p-H₂ at different temperatures, (b) 13.5 K, (c) 20 K and (d) 25 K

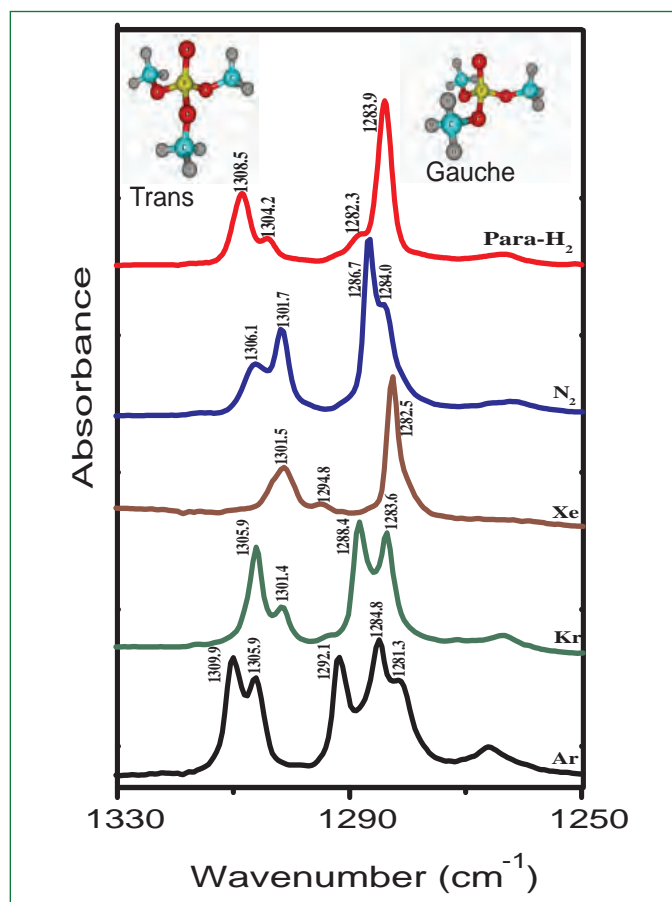


Figure 5: Infrared absorption spectra covering the P=O stretching region 1330-1250 cm^{-1} of TMP in different matrices. The structure of Gauche and Trans conformers of TMP is also shown

Figure 5 compares the matrix isolated infrared spectrum of TMP in the P=O stretching region in conventional and solid p-H₂ matrices. Simple and sharp spectral features are obtained in solid p-H₂ in comparison to conventional matrices. Other than p-H₂, xenon matrix also showed similar sharp features for TMP. The vibrational wavenumbers that occur around ~ 1285 and ~ 1305 cm^{-1} correspond to two different conformational isomers namely the 'Gauche' and 'Trans' forms of TMP with the former being the ground state and the latter is the higher energy isomer (Figure 5).

Trimethyl phosphite (TMPhite) was photo chemically oxidized to TMP in p-H₂ matrix to correlate the structural landscape of these two molecules. The infrared spectra of TMPhite recorded under isolated conditions in conventional and p-H₂ matrices revealed that it exists only in the 'Trans' form. While photo-oxidation of TMPhite in conventional matrices produced exclusively the 'Trans' conformer, the p-H₂ matrix produced both the 'Gauche' and 'Trans' conformers. Furthermore, the infrared spectra obtained through the photo-oxidation of TMPhite in p-H₂ matrix are free from spectral congestion compared to N₂ matrix (Figure 6). Clearly the simple spectrum, free from site effect is attributable to the 'quantum crystal' nature of p-H₂ and on the other hand, conventional N₂

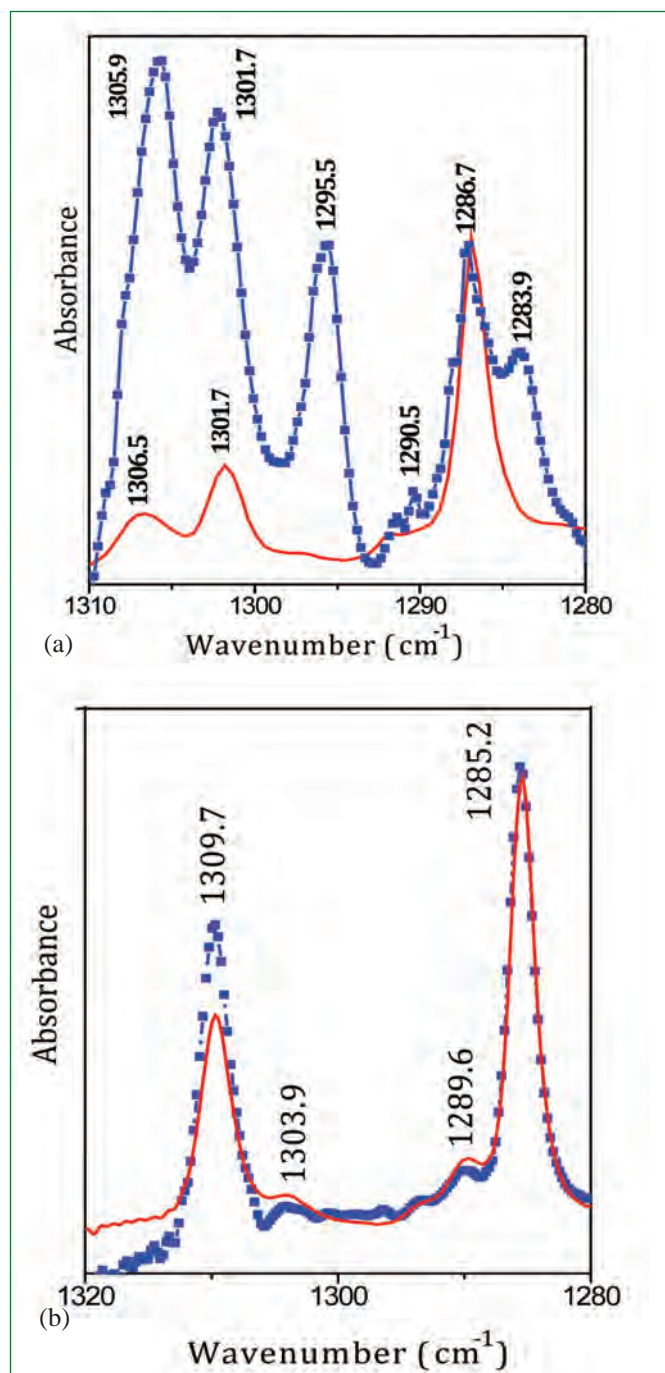


Figure 6: Infrared absorption spectra covering the P=O stretching region of TMP in (a) N₂ and (b) p-H₂ matrices. The spectra shown in red correspond to pure TMP. Shown in blue correspond to the infrared spectra of TMP produced through the photo-oxidation of TMPhite

matrix suffers severely due to the site effects. Overall, the strong site-effects of TMPhite and TMP get self repaired as the spectral features were found to be free from site-splitting in p-H₂ matrix. Certainly, experiments performed using p-H₂ gas proved it to be a promising material for matrix isolation experiments.

*Reported by
K. Sundarajan and colleagues
Materials Chemistry and Metal Fuel Cycle Group*

Non-destructive Waste Assay Computed Tomography (NDWACT) System

Towards meeting AERB safety guidelines, nuclear facilities handling radioactive materials have the responsibility of characterizing the residual radioactive content on any waste prior to disposal. The most viable approach to comply with regulatory requirement is by assessment of the long lived alpha emitting radionuclides and fission /activation of radionuclides by using Non-Destructive Assay (NDA). The results of these measurements are used for nuclear waste management, nuclear material accountability and nuclear criticality safety. The NDA technique is based on (a) passive analysis, in which, the measurement refers to spontaneous emissions of neutrons or gamma rays or to the total decay energy; (b) active analysis, in which, the measurement refers to a stimulated emission (e.g. neutron or photon induced fission).

A fully automated Waste Assay Computed Tomography (WACT) system (Figure 1) has been indigenously developed and commissioned. WACT is a high resolution gamma ray spectroscopy based transmission corrected; single photon emission computed tomography (SPECT) system. The active (transmission) and passive (emission) γ -ray computed tomography provides a solution for the assay of waste materials by combining active, passive and gamma spectroscopy and it is possible to identify, locate the distribution and quantify the special nuclear materials (SNM), transuranic (TRU) elements and fission products (FP) present inside nuclear waste drum. WACT system is capable of assaying waste containers having bulk density of up to 3 g/cc and can be operated in three modes: Tomographic Continuous Gamma Scanning (TGS), discrete TGS and Segmented Gamma Scanning (SGS) modes.

Segmented Gamma Scanning

The segmented gamma scanning is the most commonly employed technique for gamma ray assay of nuclear waste, especially for materials ^{235}U and ^{239}Pu . In segmented gamma scanning, a shielded and collimated HPGe coaxial detectors and a transmission source are used to determine attenuation of waste matrix. The transmission source and the detector are positioned at opposite sides of the drum containing waste, such that, gamma-rays from the transmission source pass through the central axis of the drum and get counted by the detector. In a typical segmented gamma scanning, drum is divided into 16 horizontal segments. For each segment, the scanning is carried out by rotating the drum in a central axis for 360° . In each segment, isotope is identified, the activity is measured separately and the total assay result is reported as sum of the activities measured from each segment. Initially, the average

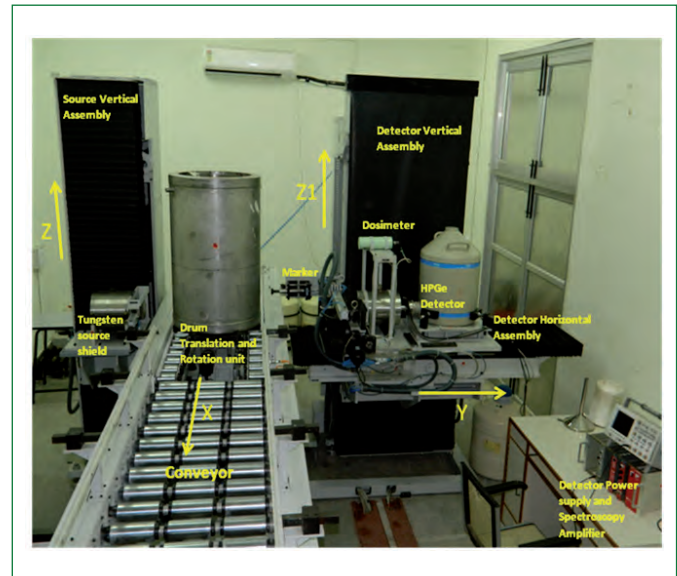


Figure 1: Waste tomography

energy dependent attenuation coefficient of each segment is determined by the transmission measurement. Then, the emission spectrum is acquired by closing the transmission source and isotopes are identified. The emission counts of each isotope are corrected using the attenuation coefficient of that emission energy for a particular layer height.

Tomographic Gamma Scanning

The assumptions in considering the uniform distribution of radioactivity and constant attenuation coefficient in a layer in segmented gamma scanning are generally not true. In tomographic continuous gamma scanning technique, individual segments are further divided into a series of volume elements (voxels) and assumed that attenuation coefficient in that voxel is constant and emission sources is distributed homogeneously in that voxel. Tomographic continuous gamma scanning is the gamma-ray-based active and passive low resolution computed tomography technique that locates, identifies and quantifies the gamma-ray emitting isotopes in nuclear waste drum. In active computed tomography (transmission computed tomography) an external radioactive source is used to scan the object and the energy dependant attenuation tomogram of scanned layer is reconstructed using Algebraic Reconstruction Technique (ART). Passive computed tomography (emission computed tomography) is used to localize and identify the specific radioactive isotope within the waste matrix. During generation of passive computed tomography, the emission counts are corrected for any overlying heterogeneous materials with the help of attenuation tomogram.



Figure 2: Simulated stainless steel waste drum filled with (a) six stainless steel rod, wooden plate at the bottom (b) cotton waste around the stainless steel tube and (c) wooden plate at the top

Passive computed tomography data are reconstructed using Maximum Likelihood Expectation Maximization (MLEM) technique.

WACT System

WACT system consists of source assembly, (¹⁵²Eu(10mCi) multi-gamma energy source as transmission source) detector assembly [50% relative efficiency HPGe Detector coupled with multi channel analyzer (MCA), waste drum translation / rotation assembly, drum lifting mechanism and associated detector electronics. Tungsten collimators are employed in front of the detector system to allow the photon from the line of site of the detector. All the motions are executed by servo motor system and they are controlled by the PLC based controller. The positioning of the drum is achieved using optical sensor system. Mechanical movement and the I/O operations are controlled by a PLC and supervisory control and data acquisition (SCADA) software. SCADA also supervises the data acquisition from MCA and motion control of servo during Tomographic continuous gamma and segmented gamma scan.

The operation of the system is completely automated using SCADA. The program in SCADA is written to operate the system sequentially as follows: To begin with it loads the drum to the conveyor system, performs translation motion, stops on pallet system, measures the weight of the drum, stamp a mark on drum at one side, measures the dose rate from the drum, lifts drum from conveyor and make the rotational motion for scanning, performs scanning either in

tomographic continuous gamma scanning or segmented gamma scanning mode based on dose rate and weight, acquires the data with respect to scan and stores in different file name. The scanning is executed with the caution that, if the dose rate is high to avoid pile-up of counts in the detector, it automatically selects the required number of attenuators. It also adjusts the position of the detector by moving the detector on Y-axis away from the drum. After the scanning, the drum is dislodged from the conveyor. The results are analysed and the tomography images are reconstructed.

Performance Experiments

Transmission and emission tomography scans are carried out with a standard size stainless steel drum of dimension 580 mm diameter and 900 mm height (volume: 210 liter). The background spectrum is taken for subtraction. At the bottom of the stainless steel drum a wooden plate with six holes is placed (Figure 2a) and six stainless steel pipes (OD: 33.7 mm and thickness of 4 mm and length of 700 mm) are inserted on each hole. Waste Cottons is filled upto 600 mm height (Figure 2b) and a wooden plate is placed on top (Figure 2c). Radioisotopes (Two ¹³³Ba , two ⁶⁰Co and one ¹³⁷Cs) are placed at different heights inside the stainless steel pipe. Source details and their positional locations are given in Table 1. For the scanning purpose the drum is horizontally split into 18 layers with an interval of 50 mm. Every layer is scanned with 33 ray-sum over 31 angles. Projection angle is 6 degree and each ray-sum spectrum is collected for 30 seconds.

The layerwise attenuation tomograms for the emission energy of 302, 355, 661, 1172, 1332 keV are interpolated from the Algebraic Reconstruction Technique generated transmission tomograms of the ¹⁵²Eu transmission energies. Using the layer wise interpolated attenuation tomogram, emission counts of the respective energies are corrected then the emission tomogram for the energy of 302, 355, 661, 1172 and 1332 keV are reconstructed by MLEM algorithm. From the neighbour hood hotspot (Figure 3a) it is determined that two sources of ⁶⁰Co are located

Table 1: Emission source location for the performance test case

S. No.	Source	Source Activity	Source position (from bottom of the drum)
1	Ba-133	92.0 μ Ci	500 mm
2	Ba-133	138 μ Ci	450 mm
3	Cs-137	1185 μ Ci	300 mm
4	Co-60	74 μ Ci	150 mm
5	Co-60	47 μ Ci	80 mm

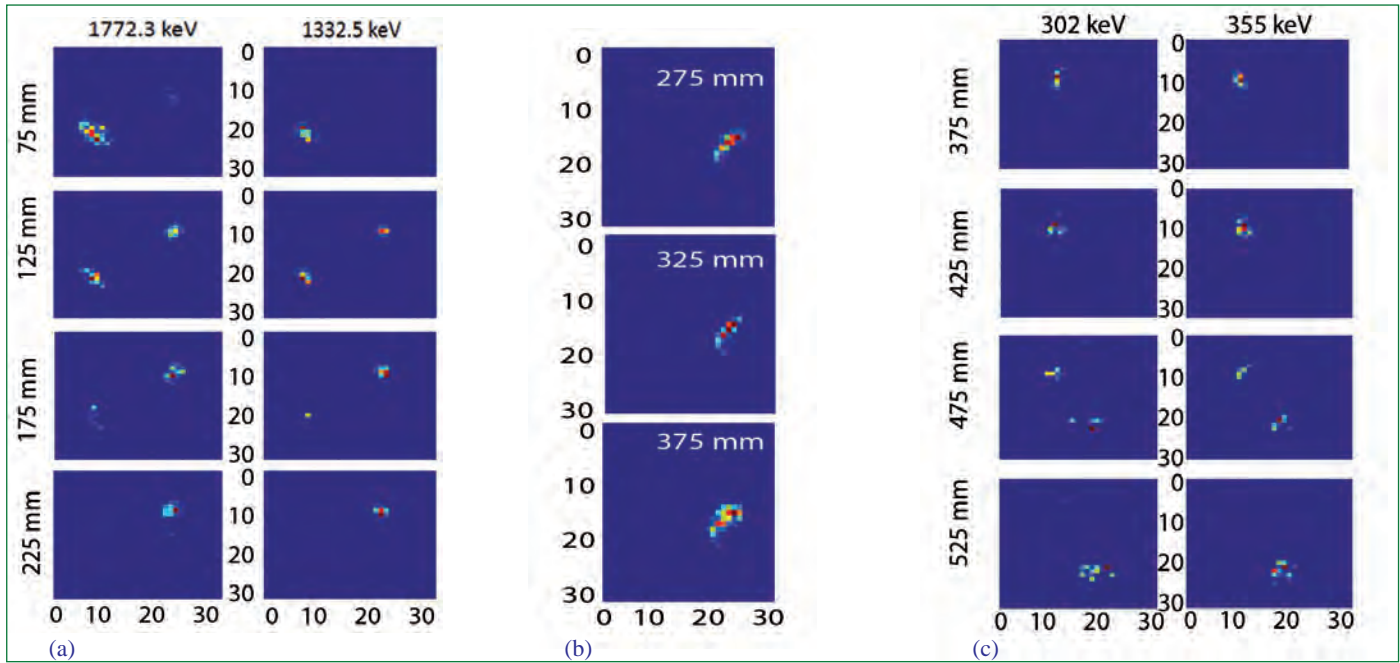


Figure 3: Emission reconstruction tomogram for the energy: (a) 1172 and 1332 keV of ⁶⁰Co source from the height 75 to 225 mm, (b) 661 Kev of ¹³⁷Cs source from the height 275 to 375 mm and (c) 302 and 355 keV of ¹³³Ba source from the height 375 to 525 mm

between a height of 75 and 125 mm and 175 and 225 mm respectively and measured activity is 79.3 and 48.4 μ Ci. From Figure 3b the hotspot sum of ¹³⁷Cs activity is calculated as 1033 μ Ci and found to be located from 375 to 525 mm. Similarly, the hotspot sum of two sources ¹³³Ba located between 375 and 425 mm and between 475 and 525 mm (Figure 3c) are identified and activity is calculated to be 87.9 and 131.1 μ Ci. Table 2 gives the details of the source location and estimated activity with % deviation in the activity measurement.

For the generation of transmission 3D image of the scanned object, all the transmission sinogram for the energy peak 344 keV is chosen, because it is predominant in the entire transmission spectrum count. The tomogram of each layer are reconstructed

S. No.	SOURCE ID	Emission Energy (keV)	Pixel Location	True activity	Measured activity	Relative Error %
1	¹³³ Ba	355	20,25	92.0	87.9	4.64
2	¹³³ Ba	355	12,10	138	131.09	5.00
3	¹³⁷ Cs	661	25,18	1185	1033	12.87
4	⁶⁰ Co	1172	9,23	74	79.36	7.24
5	⁶⁰ Co	1172	24,11	47	48.26	2.68

using Filter back projection (FBP) reconstruction algorithms from the sinogram data. During the FBP, each sinogram are interpolated for 0.1 mm with linear interpolation. Interpolated sinograms are convoluted with the Ram-Lak filter and are summed. Layer wise transmission tomograms for the energy 344 keV are stacked and the data written in VTK format as a scalar data and loaded into Visit software. Three dimensional image is reconstructed using pseudo color and iso-volume option available in the LLNL Visit 2.7.3 software. The layer wise reconstructed emission tomograms for the energies 355, 661 and 1172 keV are overlaid one by one on the transmission tomogram. The resulted image is shown in Figure 4, which reveals the locations of radioisotopes of ¹³³Ba, ¹³⁷Cs and ⁶⁰Co.

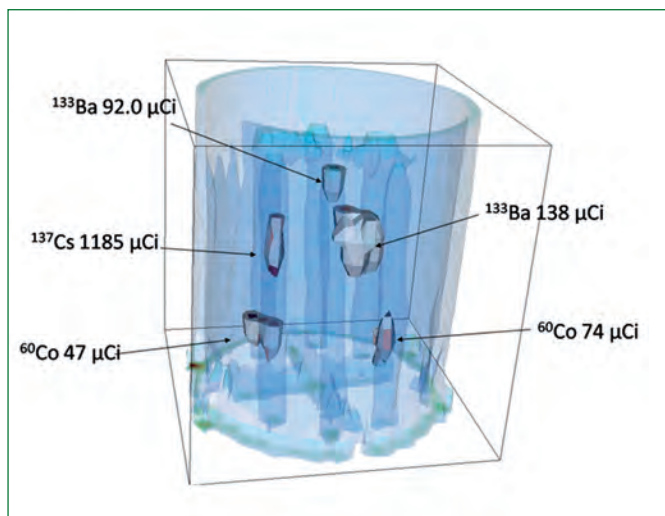


Figure 4: 3D image of the scanned object indicating source locations

*Reported by
R. Ramar and colleagues
Health, Safety and Environment Group*

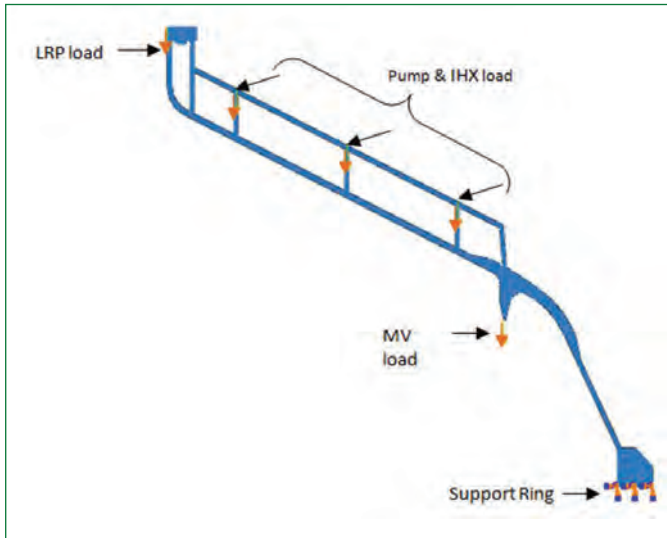


Figure 3: Roof slab model with loading details

Estimation of Fatigue Load

Large thermal stresses are generated in the tri-junction joint region due to significant thermal gradient across the joint. Further, this joint region experiences fluctuating temperature cycles between normal reactor operation and SGDHR (Safety Grade decay Heat Removal System) condition. This varying temperature cycle imposes fatigue to the joint. In addition to these varying thermal stresses, mechanical stresses also exist in the tri-junction due to the loads acting on the roof slab as well as main vessel load. Hence, structural and thermal analyses are carried out to arrive at the fatigue load.

Structural Analysis of Tri-junction

Description of the finite element model

The modelling and finite element analyses are done using ABAQUS FE analysis software. Since the geometry is symmetric about vertical axis Axi-symmetric modelling is used for analysis. The element used to mesh the component is 4 noded bilinear axi-symmetric quadrilateral element (CAX4R) with two degree of freedom at each node: translations in the r and z directions. In order to simulate the exact loading condition, the roof slab is also modelled (Figure 3).

Analysis results

Structural analysis is performed for tri-junction. Figure 4 shows the Von Mises stress distribution of tri-junction. The local Primary membrane stress (P_L) is found to be 37 MPa, at the bottom section of the tri-junction. Since thermal stresses are observed to be maximum at the bottom section of tri-junction, the same location is considered for estimating Primary membrane stress (P_L).

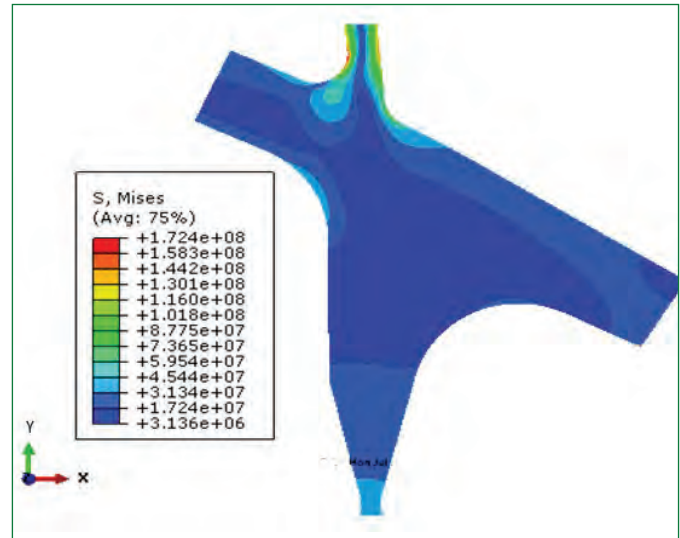


Figure 4: Von Mises stress at Tri-junction under normal operating condition (in Pa)

Thermal Analysis of Tri-junction

Temperature distribution and boundary condition

The element used to mesh the component is 8 noded axi-symmetric quadrilateral, bi quadratic element (CAX8T). The temperature values extracted from the integrated thermal analysis of top shield and reactor vault under normal and SGDHR conditions are used for the thermal analysis. Fixed boundary condition is applied on the support ring.

Thermal stress analysis

The stress distribution of the tri-junction for normal operating condition is shown in Figure 5. The maximum stresses (ΔQ_{max}) in the tri-junction for the normal and SGDHR conditions are 327 and 502 MPa respectively. The high thermal stresses at the tri-junction are due to the large thermal gradient along the vertical direction of tri-junction.

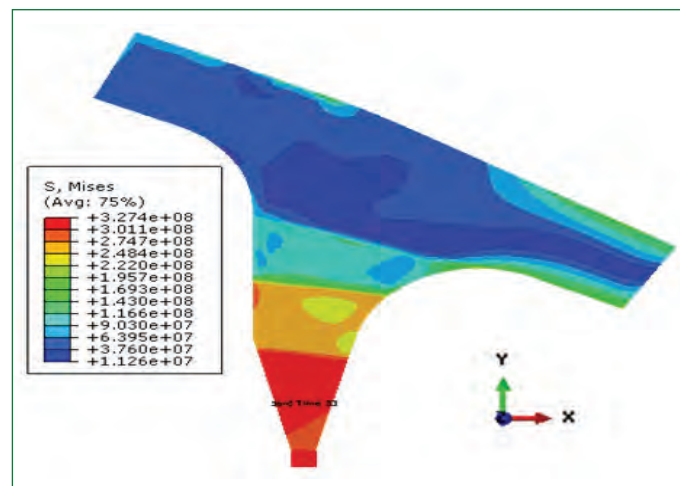


Figure 5: Thermal stress at tri-junction under normal operating condition (in Pa)

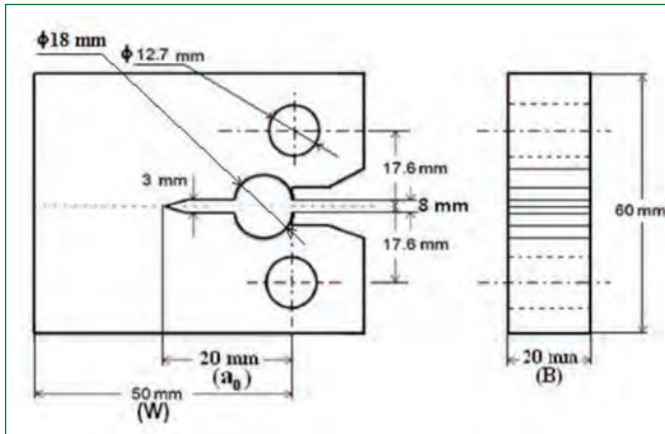


Figure 6: Geometry and dimension of CT specimen

Fatigue load calculation

Efficiency index method is used to calculate the effective stress as the component is subjected to both primary (mechanical load) and secondary (thermal) stresses. Maximum effective stress (σ_1) and minimum effective stress (σ_2) are found to be 110 and 137 MPa respectively, as per RCC-MR. Stress intensity factors (K_1 and K_2) corresponding to maximum and minimum stress are calculated as 27.57 and 34.34 MPa \sqrt{m} respectively. Similarly, maximum load (P_1) and minimum load (P_2) corresponding to K_1 & K_2 are calculated as 21.41 and 17.18 kN respectively. From this, fatigue load is estimated as 4.217 kN and the load ratio is found to be 0.8. These values are used in the Fatigue Crack Growth (FCG) rate experiment.

Experimental Estimation of Fatigue Crack Growth Rate

Specimen material

SS 304L is the material for tri – junction in the reactor. But in the present work, carbon steel (IS 2062) specimens are used for experiment as carbon steel forged blank was readily available. This is also justified considering the objective of study i.e., comparison of structural integrity of forged and welded material for the joint. Further, use of carbon steel for the present study leads to conservatism as the crack propagation rate of carbon steel is higher than SS 304L, owing to their marked difference in ductility values. The experiments are conducted at room temperature (300 K) and high temperature (623 K) to compare the crack propagation behaviour at different temperature conditions. During SGDHR condition, the temperature of the tri junction is 623 K and the same was chosen for experiment.

Specimen Preparation

Compact Tension (CT) specimens with nominal thickness $B = 20$ mm, and width $W = 50$ mm were prepared as per ASTM E647 from forged carbon steel blanks (Figure 6). The notch (~ 20 mm)

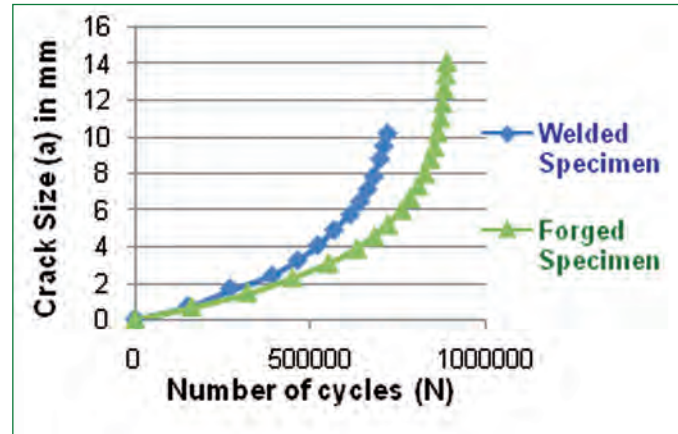


Figure 7: Crack size (a) Vs Number of cycles (N)

is cut using wire EDM (with an included angle of 45°). Welded specimens are fabricated from carbon steel plates using manual metal arc welding with E7018 electrode. Butt welding with a root gap of 10 mm (using back strip) is adopted for obtaining weld metal region of sufficient width.

Fatigue pre-cracking

Prior to Fatigue Crack Growth test, the CT specimens are subjected to the fatigue pre-crack, i.e. a crack of length 2–3 mm is introduced at the notch in order to achieve the a/W ratio as per the ASTM E647 guidelines. This pre-cracking provides a sharpened fatigue crack of adequate size and straightness which ensures that the effect of the machined starter notch is removed from the specimen.

FCG test

All the FCG tests are conducted in accordance with the requirement of ASTM E647 at room temperature and high temperature (623 K) conditions. Fatigue load of 4.217 kN and constant load ratio $R = 0.8$ is used for the test. ΔK increasing procedure is adopted to conduct all the tests. Crack lengths are measured online using a suitably calibrated direct current potential drop (DCPD) system. The results from this test are obtained in terms of crack length (a) and number of cycles (N). From this, crack growth rate is calculated using seven point incremental polynomial method as per the ASTM E647 guidelines. Using the values of crack length and corresponding load, ΔK is calculated.

Experimental Results and Discussion

Fatigue crack growth test

The number of cycles for normal operation – SGDHR conditions is 1000. Thus, crack sizes after 1000 cycles (a_{1000}) are estimated from experiments for both welded and forged specimens at room temperature as well as high temperature conditions. From Crack size (a) Vs number of cycles (N) graph obtained from experiments (Figure 7), crack growth rate (da/dN) is calculated as per ASTM E 647 guidelines. Using the values of crack length and

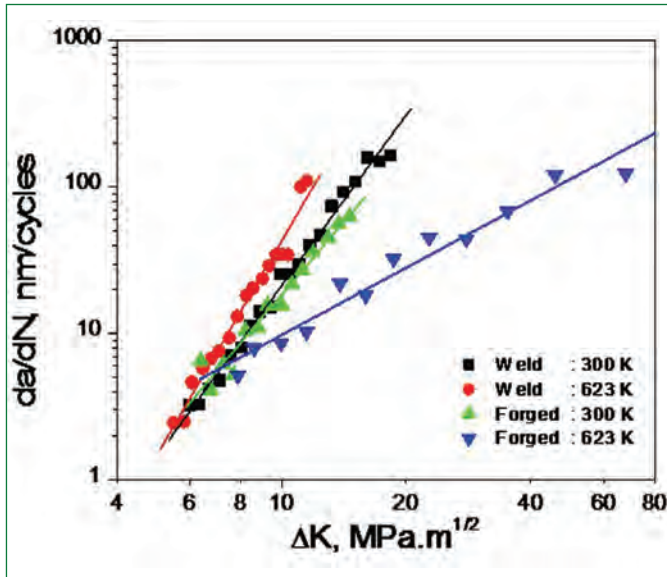


Figure 8: Fatigue Crack Growth rate of welded & forged CT specimens

fatigue load, ΔK is calculated. Using the above values, da/dN Vs ΔK graphs for welded and forged CT specimens at different temperatures are plotted and presented in the Figure 8. Paris law constants 'c' (intercept in da/dN Vs ΔK curve) and 'm' (slope in da/dN Vs ΔK curve) are estimated from da/dN Vs ΔK graphs. The following observations are made:

- At high temperature and higher ΔK , Fatigue Crack Growth rate of forged specimen is found to be lower compared to welded specimen
- At lower ΔK , irrespective of the temperature, Fatigue Crack Growth rate of welded as well as forged specimen is found to be more or less same
- In general, Fatigue Crack Growth rate of forged specimen is lower than the welded specimen

Remaining life of the component beyond design life

Remaining life of the component is nothing but the number of cycles the component takes to reach its critical crack size beyond design life. It is calculated using the following equation.

$$\int_{a_{1000}}^{a_c} \frac{da}{dN} = \int_0^N c(\Delta K)^m ; N = \int_{a_{1000}}^{a_c} \frac{da}{c(\Delta K)^m}$$

where, a_{1000} is crack size after 1000 cycles and is taken from experiments, a_c is critical crack size corresponding to fracture toughness, c is intercept and m is slope in da/dN Vs ΔK curve, ΔK is SIF range and it is function of crack size, K_{Ic} is fracture toughness and it is referred from RCC-MR.

Using the values of c , m , a_{1000} , a_c and K_{Ic} for forged (RT), welded (RT), forged (HT) and welded (RT), remaining life of the specimens is estimated and the same is presented in Table 1. It is clear that the remaining life of the forged specimen is higher than the welded specimen. But remaining life of the forged specimen at high temperature is higher than at room temperature. The higher crack growth rate of the forged specimen at room temperature when compared to high temperature, can be attributed to the presence of residual stresses in the specimen, as the forged piece was not stress relieved after forging. However, when the same specimens are tested at high temperature, due to relieving of residual stresses, the crack growth rate is reduced. But in reactor, annealed SS304L material will be used for roof slab. So, the effect of residual stress is expected to be insignificant.

Estimation of Structural Reliability

Structural reliability of a component is estimated using reliability index (β). A limit state function (g) is defined in terms of strength (S) and loading (L) on a structural component as $g = S - L$. Hasofer Lind reliability index method is used to find β as the limit state function is non-linear. The strength parameter is fracture toughness and the load parameter is Stress Intensity factor (SIF) range. These basic variables account for the uncertainties in the load, material property and geometry etc. Fracture toughness (K_{Ic}), crack size (a) and fatigue load (ΔP) are considered as variables. Distribution, standard deviation and coefficient of variation are referred from literature. Coefficient of variation of fatigue load, crack size and

Table 1: Remaining life of the specimens

Specimen	c (m /cycle)	m	a_{1000} (mm)	K_{Ic} (MPa√m)	a_c (mm)	Remaining Life of the specimen beyond design life (No. of cycles to failure)
Welded (RT)	2.89×10^{-12}	3.876	0.756	109	44.8	2.98×10^6
Forged (RT)	8.73×10^{-12}	3.310	0.565	145	45.6	1.475×10^7
Welded (HT)	5.96×10^{-13}	4.857	0.891	102	44.6	1.69×10^5
Forged (HT)	2.89×10^{-13}	1.530	0.387	136	45.5	6.44×10^8

fracture toughness varies between 0.01-0.1, 0.1-0.2 and 0.01-0.1 respectively. Coefficient of variation of crack size is high compared to other variables as it involves more uncertainties. Conservatively, higher values of coefficient of variation are taken for variables.

Estimation of Reliability Index (β)

The steps involved in the Hasofer Linde method to find β are explained below.

Step: 1

Limit state function is defined in terms of fracture toughness (strength) and stress intensity factor (load).

$$g = \Delta K_{IC} - \frac{\Delta P (2+\alpha)(0.866+4.64\alpha-13.32\alpha^2+14.72\alpha^3-5.6\alpha^4)}{B\sqrt{W}(1-\alpha)^{1.5}}$$

Step: 2

Variables involved in the estimation of SIF range are transformed into normal standard space to include the uncertainties present in the material, mechanical and loading conditions. The transformed variables are shown below.

$$K_{IC} = \mu_{K_{IC}} + \sigma_{K_{IC}} u_{K_{IC}} ; a = \mu_a + \sigma_a u_a ; \Delta P = \mu_{\Delta P} + \sigma_{\Delta P} u_{\Delta P}$$

where $\mu_{K_{IC}}$, μ_a and $\mu_{\Delta P}$ are mean values of fracture toughness, crack size and fatigue load range respectively $\sigma_{K_{IC}}$, σ_a and $\sigma_{\Delta P}$ are standard deviation of fracture toughness, crack size and fatigue load range respectively.

Step: 3

Initially, the values of $u_{K_{IC}}$, u_a and $u_{\Delta P}$ are assumed to be zero. i.e., mean values of variables are considered for the first iteration.

$$u_{K_{IC}} = u_a = u_{\Delta P} = 0$$

Step: 4

Partial derivatives of limit state function w.r.t. each random variables are found for estimating β .

i.e. $\frac{\partial g}{\partial u_{K_{IC}}}$, $\frac{\partial g}{\partial u_{\Delta P}}$ and $\frac{\partial g}{\partial u_a}$ are found

Step: 5

$u_{K_{IC}}$, u_a and $u_{\Delta P}$ values are found using the formula given below. Partial derivatives calculated in the above step are used in the formula given below.

$$u_i = \frac{\frac{\partial g}{\partial u_i} \sum_{i=1}^n \frac{\partial g}{\partial u_i} u_i - g}{\sum_{i=1}^n \left(\frac{\partial g}{\partial u_i} \right)^2}$$

Step: 6

Reliability index is calculated using the formula given below.

$$\beta = \sqrt{u_a^2 + u_{K_{IC}}^2 + u_{\Delta P}^2}$$

Step: 7

$u_{K_{IC}}$, u_a and $u_{\Delta P}$ values calculated in step 4 will be used in the next iteration. The iteration is continued till the β value converges.

Step: 8

Probability of failure is calculated using,

$$P_f = \phi(-\beta)$$

The probability of failure of forged (RT), welded (RT), forged (HT) and welded (HT) specimens for corresponding β values are 4.433×10^{-19} , 5×10^{-19} , 7×10^{-19} and 1.06×10^{-18} respectively. From the above values, it is clear that the probability of failure of forged specimen is lower than the welded specimen. Thus, it is concluded that the reliability of the forged component is better than the welded component.

In the proposed dome shaped configuration for roof slab of future FBRs, the tri-junction joint between roof slab, main vessel and roof slab support can be designed either as a forged joint or as a welded joint. In this context, it is proposed to compare the structural reliability of the above two options. Towards this, fatigue load is calculated first using structural and thermal analyses of tri-junction (by FE analysis software) for normal operation & SGDHR conditions. Using the above calculated fatigue load, experiments are conducted to measure the FCG rates, as per the standard ASTM E647 under room temperature (300 K) as well as at high temperature (623 K). Crack sizes and Paris law constants obtained from the experiments are used for estimating the remaining life of the specimen beyond design life. Subsequently, structural reliability of the forged and welded specimen are estimated corresponding to 1000 cycles (a_{1000}) using Hasofer Lind's method.

It is seen that the remaining life of the forged specimen beyond design life is three order higher than the welded specimen. Also, the remaining life of the forged specimen at high temperature is higher than the room temperature. From the reliability analysis, it is clear that the probability of failure of forged specimen is one order lower than the welded specimen and the probability of failure of forged specimen at high temperature is least. Thus, through analytical and experimental approaches, it is concluded that the reliability of the forged joint is better than the welded joint.

*Reported by
V. Vinoth and colleagues
Reactor Design Group*

Young Researcher's FORUM

Effect of Impurities on Physicochemical Properties of Group III Nitride Nanowires

GaN nanowires can be grown using almost all the thin film deposition techniques namely molecular beam epitaxy (MBE), organometallic vapor phase epitaxy (OMVPE) and different types of chemical vapor deposition (CVD) methods. MBE growth can produce GaN with ultimate phase purity and crystal quality but is economically challenging. CVD, on the other hand, can be used for large scale production in a cost effective way. However, oxygen impurity in CVD growth is a concern. Although, the effect of oxygen impurity on several characteristics of GaN thin films was studied earlier, its influence on the morphology, particularly 1D nanostructures is not known. The reproducibility and homogeneity of required size and morphology of GaN nanowires in a simple CVD technique are critical issues for mass production of ensemble nanowire devices. Controlling diameter and surface morphology of GaN nanowires play a crucial role in defining physicochemical properties including electrical, optical, electrochemical and electromechanical properties for large scale production of the nanowire devices. In this context, we have studied the effect of oxygen impurity on morphological, structural, optical and chemical characteristics of nonpolar (*m* and *a*-axes oriented) GaN nanowires grown using atmospheric pressure chemical vapor deposition (APCVD) technique via vapor-liquid-solid process (VLS). The wurtzite crystal of III-nitrides grown along the *c*-axis; [0001] is



Shri Avinash Patsha did his Masters in Physics from Banaras Hindu University, Varanasi. He joined IGCAR as a DAE research fellow in Physical Sciences in August 2010 and carried out his doctoral work in the Surface and Nanoscience Division, MSG, under the guidance of Dr. Sandip Dhara. His doctoral thesis entitled "Effect of Impurities on Physicochemical Properties of Nonpolar GaN Nanowires" has been submitted to Homi Bhabha National Institute. His research interest includes physics and chemistry of semiconductor nanowires, transport in 1-D nanostructures, III-N nanowires.

called polar while *m*-axis; [10-10] and *a*-axis; [11-20] are called non-polar.

Growth of GaN Nanowires via VLS Process

The APCVD process involves the formation of a solid film on a heated substrate surface by means of generation, transport, absorption and chemical reactions of vapor phase reactant species at atmospheric pressure. A complete experimental setup of custom-built APCVD system (Figure 1a) has been developed for the growth of GaN nanowires. The growth of GaN nanowires has been carried out in VLS process using the optimized Au nanoparticles of size $30(\pm 5)$ nm as catalyst on Si substrate, Ga metal (5N) as precursor, NH_3 (5N) as reactant gas, and a mixture of ultra high pure (UHP) $\text{Ar} + \text{H}_2$ (5N) as carrier gases. With optimized growth parameters such as growth temperature (900 °C), flow rates of reactant (10 sccm) and carrier (20 sccm) gases, GaN nanowires having smooth and homogeneous surface morphology and uniform size distribution with diameter of $40(\pm 5)$ nm (Figure 1b) are grown. The particle at the tip suggests that the

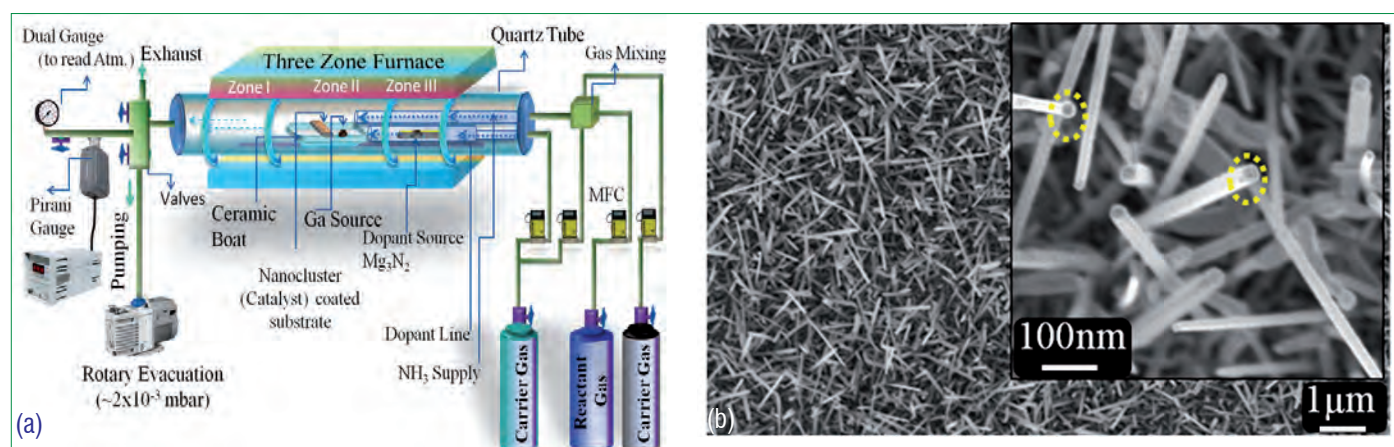


Figure 1: (a) Schematic view of the APCVD system used for growth of GaN NWs and (b) typical FESEM micrograph of GaN NWs. Inset shows the high magnification micrograph

growth of nanowires followed the VLS process. We have also succeeded in obtaining required size and reproducibility of the growth of nanowires by tuning the size of the Au catalyst particles.

Impurity Effect on Morphological and Structural Characteristics

For studying the effect of oxygen impurity, GaN nanowires were grown under different concentrations of oxygen impurity in the range of 1.2×10^{-4} Torr (< 2 ppm) to 1.3×10^2 Torr (10^5 ppm). The typical morphologies of the as-grown nanowires were studied using Field emission-Scanning electron microscope (FESEM). The nanowires of sample R1 (Figure 2a) and R2 (Figure 2b), grown under oxygen rich atmospheres of 10^5 and 10^3 ppm, respectively, are found to be quite rough with non-uniform surface morphologies along the wires. These nanowires have a large diameter distribution of 40–150 nm, but majority of them have < 60 nm diameter. The diameter distribution of nanowires of sample R3 (Figure 2c), grown under 10^2 ppm of oxygen is reduced to 40–100 nm. The nanowires R4 (Figure 2d), grown under oxygen deficient atmospheres, showed uniform shape with homogeneous surface morphology and a narrow diameter distribution of $\sim 60(\pm 15)$ nm. The uniform size and homogeneous morphology of the nanowires, might be a result of the controlled and thermodynamically stable growth of the crystallites with specific crystalline orientation of pure GaN phase by the incorporation of Ga and N species during the growth process. The study revealed the degradation in the surface morphology, uncontrollable growth rate and size variations of nanowires as a consequence of oxygen impurity incorporation in nanowires during the growth.

The structural studies of the nanowire samples were carried out using transmission electron microscope (TEM) to understand growth mechanism. The diffraction spots enclosed by dotted circles in FFT image (inset of Figure 3a) corresponding to high resolution TEM (HRTEM) micrograph of the nanowire (Figure 3a), are indexed to $\{10\bar{1}0\}$ and $\{0002\}$ planes of wurtzite GaN phase. Lattice fringes with d -spacing of 0.275 nm corresponding to $\{10\bar{1}0\}$ planes of GaN phase are observed. While for nanowire of R4, the SAED pattern (inset of Figure 3b) revealed that the nanowire is a single crystalline wurtzite phase of GaN with zone axes $[0001]$. An interplanar spacing of 0.275 nm (Figure 3b), corresponds to the nonpolar $\{10\bar{1}0\}$ planes of wurtzite GaN are clearly seen. The growth direction of the nanowire is found to be along $[10\bar{1}0]$ direction. The study conforms that the growth of nanowires under oxygen free environment resulted in a single crystalline nonpolar GaN nanowires with uniform shape along the wire. Whereas, the growth under oxygen rich atmosphere (R1) results in the nanowires having crystalline planes of wurtzite GaN oriented in different directions along with an amorphous layer

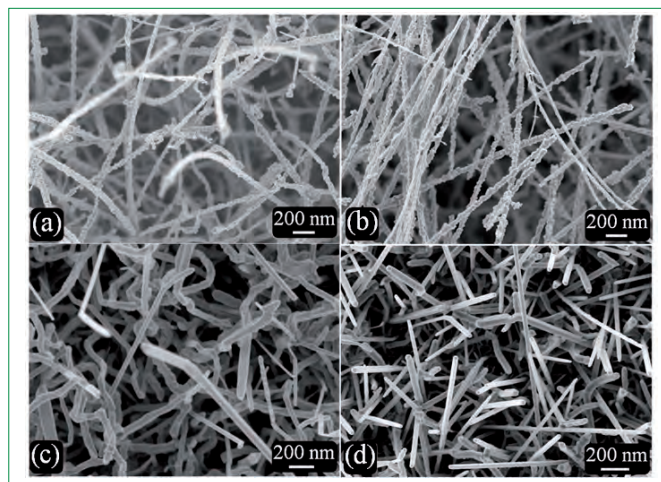


Figure 2: Typical FESEM micrographs of GaN nanowires grown under different oxygen concentrations (a) sample R1, (b) sample R2, (c) sample R3 and (d) sample R4

covered inhomogeneously on the nanowire surface.

In order to confirm the existence and variations in oxygen impurity concentrations in the nanowires, we have carried out electron energy loss spectroscopy (EELS) studies in-situ during TEM observations. The EELS spectra of nanowires of the four samples were analyzed by collecting the K -edge emission of N and O. The spectra show a drastic variation in the fine structures of N- K and O- K edges. The variation in the N to O concentration (n_N/n_O) with respect to nanowire surface morphology was investigated by obtaining the EELS spectra at different positions along a single nanowire. The ratio (n_N/n_O) is found to vary between 0.09 - 0.2 for nanowires of R1. While for nanowires of R4, hardly any variation (1.19-1.21)

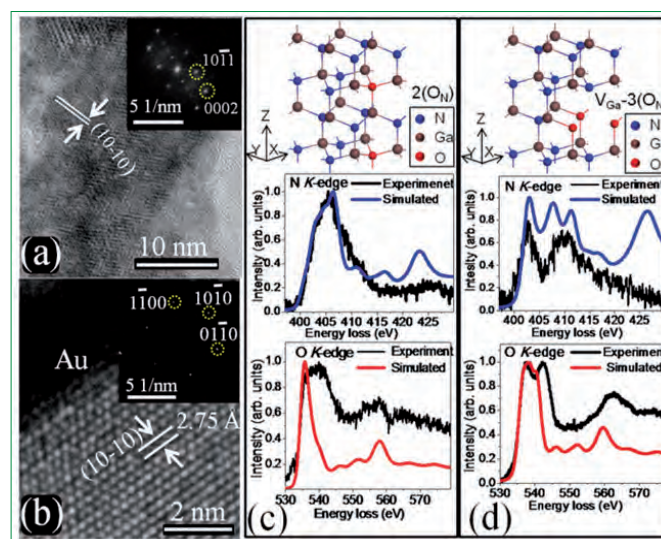


Figure 3: (a) and (b) Typical HRTEM micrographs of the nanowires from sample R1 and R4, respectively. Insets show corresponding FFT images. (c) Comparison of experimental and simulated EELS spectra of nanowires from sample R3 with $2(O_N)$ defect configuration and (d) nanowires from sample R1 with $V_{Ga}-3(O_N)$ defect configuration

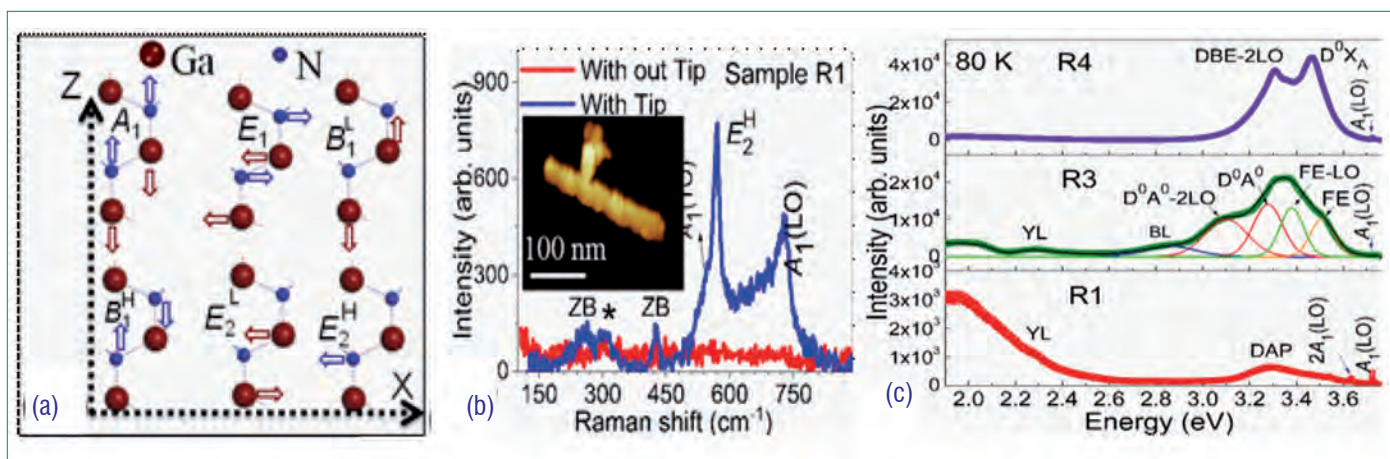


Figure 4: (a) Schematic view of the atomic vibrations in wurtzite GaN. (b) TERS spectra of a single GaN nanowire of R1 with and without TERS tip. AFM image of the nanowire is shown in inset. (c) PL spectra of GaN nanowires

was observed. The data showed the inhomogeneous incorporation of oxygen into the crystalline planes of GaN. Further, we simulated the EELS spectra of different oxygen impurity defect complexes in GaN structure using density functional theory calculations and correlated with experimental data (Figures 3c and 3d). The study showed that the most favorable defect complexes $2(\text{O}_\text{N})$ and $V_{\text{Ga}}\text{-3O}_\text{N}$ of GaN are present in the O-rich nanowires. From the morphological and structural studies of nanowires, growth and O-impurity incorporation mechanisms have been explained.

Effect on Optical Properties

The incorporation of impurities in the nanowire modifies the optical properties along with structural variations. The effect of impurity on optical characteristics of GaN nanowires was studied using Raman and Photoluminescence (PL) spectroscopy. The atomic vibrations in wurtzite GaN for zone centre phonons are shown schematically in Figure 4a. In order to observe the localized effect of impurities in nanowires, Raman spectra from a single nanowire of R1 was recorded in the sub-diffraction limit using tip enhanced Raman spectroscopy (TERS). The observed E_2^L , $A_1^L(\text{TO})$, E_2^H and $A_1^L(\text{LO})$ phonon modes corresponds to wurtzite GaN (Figure 4b). The zone boundary (ZB) phonon modes due to the finite crystallite size effects and surface optical (SO) phonons of GaN are also observed. A tiny peak corresponding to oxy-nitride (GaO_xN_y) phase observed in TERS spectrum suggests the impurity phase formation in nanowires due to oxygen incorporation.

The optical quality of the GaN nanowires was investigated by collecting PL spectra. The luminescence from the nanowires of R1 (Figure 4c), showed a broad emission around 2.0-2.3 eV (Yellow luminescence; YL) and ~ 3.27 eV (donor-acceptor pair; DAP). In GaN, oxygen easily substitutes the N (O_N) due to low defect formation energy and forms a shallow donor level. The Ga

vacancies (V_{Ga}) are deep acceptors and forms complexes with oxygen shallow donors as $V_{\text{Ga}}\text{O}_\text{N}$, which causes the emission of the YL band around 2.2 eV. An increase in the intensity of the YL band with oxygen-impurity in nanowire samples confirm the presence of $V_{\text{Ga}}\text{O}_\text{N}$ defects. Emission due to excitons bound to neutral donors (D^0X_A), which is commonly peaked at 3.47 eV, is completely suppressed. This shows that the optical quality of nanowires (R1) grown in oxygen rich condition is degraded. The absence of the YL band and strong emission of DX band in luminescence spectra of nanowires (R4) grown under the oxygen reduced condition are the implication of high optical quality GaN phase.

Effect on Sensing Properties

Usually, for chemisorbed species during the sensing process, the charge transfer on a semiconductor surface is driven by the active sites available on the surface. The active sites are governed by intrinsic and extrinsic defects in semiconductors, metal-semiconductor Schottky junctions or some functional groups attached to the surface. Thermally stable and chemically inert pure group III-nitride semiconducting surfaces (such as GaN and AlGaN) utilize the Schottky junction formed by metal contact or heterojunctions with other semiconductors as active sites. Several earlier studies pointed out that the origin of sensing response by III-nitride nanowires without assistance of metal particles could be due to oxygen impurities. However, the underlying mechanism was not clear. In this context, by utilising a state-of-the-art facility (Multi-probe SPM), we have studied and explored the charge transfer mechanism in CH_4 sensing by GaN nanowires without any Schottky junctions.

The gas sensing responses by the GaN nanowires (samples R1, R2, R3 and R4) towards CH_4 , were tested in the temperature range of 50 to 150 $^\circ\text{C}$. The devices of sample R1, R2 and R3 showed

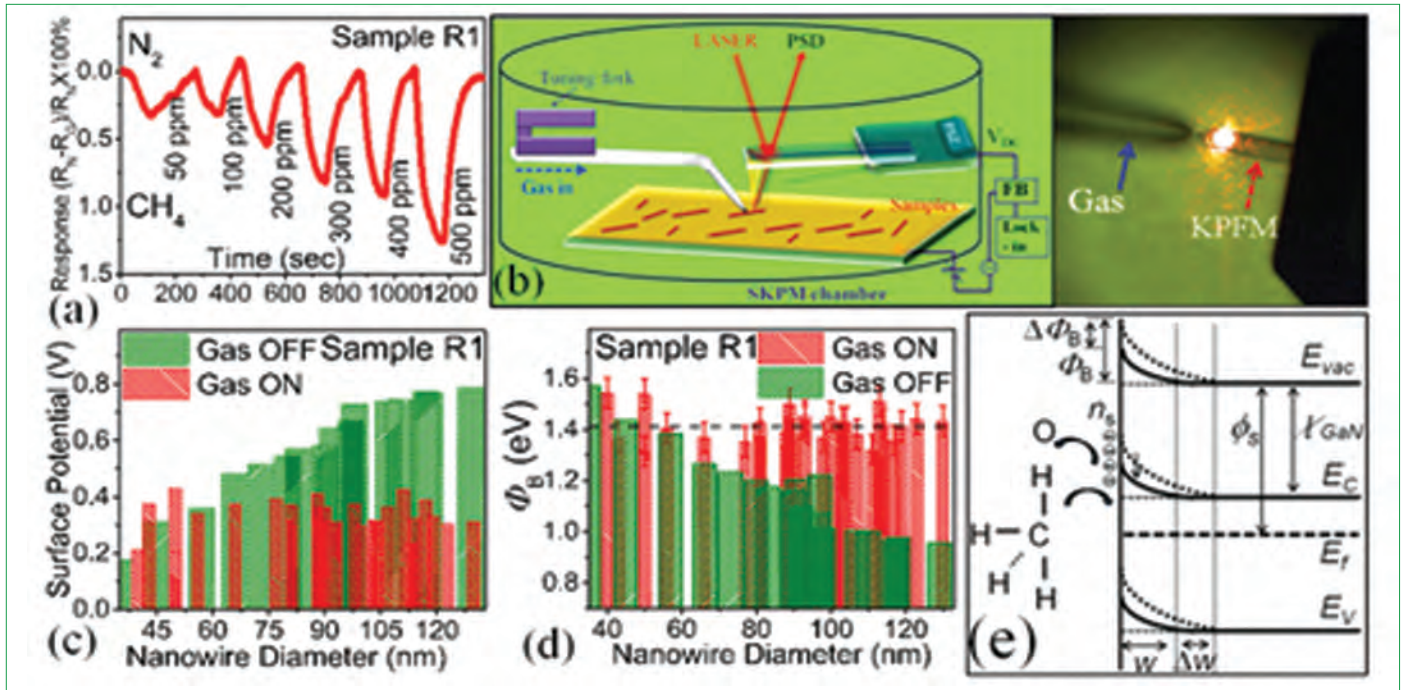


Figure 5: (a) Temporal sensing response by GaN nanowire samples R1, (b) Schematic view of the SKPM setup (left side) and an optical image of aligned two probes (right side). (c) nanowire diameter dependent SP values extracted from the SKPM maps of sample R1 before (gas OFF) and during the CH₄ exposure (gas ON). (d) and (e) nanowire diameter dependent SBB (ϕ_B) and its schematic view in nanowires during CH₄ sensing

significant responses even for low concentration of 50 ppm gas exposure at 125 °C (Figure 5a) and the response decreases from R1 to R3 (1.27 to 0.54 %). In contrast, the device of R4 did not respond even for 500 ppm. The observed responses by the nanowire samples suggested the role of oxygen defect complexes 2(O_N) and V_{Ga}-3O_N as active sites for the chemisorption of CH₄. During the sensing process, the chemisorbed molecules on semiconductor surface induce a bending of energy bands near the surface. This surface band bending;

$$SBB (\Phi_B = \phi_M - qV_{CPD} + \phi_{off} - \chi + (E_c - E_f))$$

can be precisely studied by the scanning Kelvin probe microscopy (SKPM) technique by measuring surface potential (SP) or the contact potential difference (CPD) ($V_{CPD} = (\phi_M - \phi_s) / q$) on the Nanowires. Here, ϕ_M , ϕ_s , and χ are work functions of metal and semiconductor, electron affinity of semiconductor respectively. Apart from the adsorbed gas or chemical molecules, SBB also depends on type of semiconductor, intrinsic and extrinsic defects and nanowire diameter. The GaN Nanowire diameter and oxygen impurity dependent SP measurements, prior to CH₄ exposure, showed the increase in SP values with increase in diameter and oxygen impurity (R4 to R1 for fixed diameter). In order to understand the charge transfer process during the gas sensing, *in situ* SKPM (Figure 5b) measurements at 100 °C and 10⁻² mbar in dark were carried out on single GaN Nanowires under CH₄ exposure.

A negligible change in the SP ($\Delta V_{SP} = 5$ to 17 mV) values of before and during the CH₄ exposure was observed for R4, while for R1, ΔV_{SP} varied between -150 to +460 mV (Figure 5c). By considering large variations in SP of R1, we have estimated SBB (Φ_B) of R1 before (1.57 - 0.95 eV) and during (saturated at $\sim 1.41 \pm 0.06$ eV) the CH₄ exposure over a range of Nanowire diameters of 35 - 130 nm (Figure 5d). Below a critical diameter of ~ 60 nm, Φ_B is decreased by an amount of 0.16 eV due to the CH₄ exposure. The decrease in Φ_B indicates that the decrease in surface charge density (n_s), depletion width

$$\{W = (n_s / N_D) = (2 \Phi_B \epsilon \epsilon_0 / q^2 N_D)^{1/2}\},$$

and hence the resistance of the Nanowire during the CH₄ exposure (Figure 5e). The analysis of SBB thus helped in understanding the localized charge transfer process in single GaN Nanowire, involving V_{Ga}-3O_N defect complex which controlled the global gas sensing behavior of the oxygen rich GaN nanowire ensemble during CH₄ sensing.

The results of this study provided an insight for controlling the impurities and thus defects associated with impurities in III-nitride based nanowires for advanced electronic, optoelectronic and sensor device applications.

*Reported by
Avinash Patsha and colleagues
Materials Science Group*

News & Events

Graduation Function of the 10th Batch of Trainee Scientific Officers of BARC Training School at IGCAR

July 29, 2016



Dr. A. S. Kiran Kumar, Dr. Arun Kumar Bhaduri, Dr. M. Sai Baba and Dr. Vidya Sundararajan during the release of souvenir at the graduation function

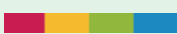
The 10th batch of thirty seven Trainee Scientific Officers from the BARC Training School at IGCAR have successfully completed their training and were graduated in a special ceremony that took place on July 29, 2016. Dr. A. S. Kiran Kumar, Chairman, Indian Space Research Organisation, Department of Space, Government of India was the Chief Guest. Dr. M. Sai Baba, Director, Resources Management Group welcomed the gathering. Dr. A.K. Bhaduri, Distinguished Scientist and Director, IGCAR delivered the presidential address. Dr. A.S. Kiran Kumar released the souvenir featuring the training school programme during the academic year and its successful completion of ten years. Dr. Kiran Kumar gave away the

prestigious 'Homi Bhabha Prizes' comprising of a medallion and books worth Rs. 5000 to the toppers from each discipline and addressed the gathering. He also gave away the course completion certificates to all the graduates passing out. A few of the Trainee Scientific Officers passing out shared their experience, gave a feedback on the academic programme and their stay at the hostel. Dr. Vidya Sundararajan, Head, Strategic Planning and Human Resource Development Division, Resources Management Group, proposed the vote of thanks.

*Reported by
M. Sai Baba,
Director, RMG*



Graduates of BARC Training School at IGCAR with Dr. A. S. Kiran Kumar, Chairman, Indian Space Research Organization, Dr. Arun Kumar Bhaduri, Director, IGCAR, and senior colleagues of the Centre and the Department

News & Events 

BITS Practice School

May 23 - July 16, 2016



Dr. Arun Kumar Bhaduri, Director, IGCAR distributing certificates to the participants during the valedictory function

Fifty one students from BITS Pilani, Hyderabad and Goa campuses underwent Summer Practice School at our Centre during May 23-July 16, 2016. This programme is aimed at exposing the students to industrial and research environments, how the organizations work, to follow and maintain work ethics, study the core subjects and their applications in the organization, participate in the assignments given to them in the form of projects. Dr. S.A.V. Satya Murty, the then Director, IGCAR inaugurated the Practice School programme and interacted with the students. The students were from various disciplines like Chemical Engineering, Computer Science & Engineering, Electrical & Electronics Engineering, Electronics & Instrumentation Engineering, Mechanical Engineering

and Physics. Dr. Michael Alphonse, BITS Practice School Division, Hyderabad Campus was the programme coordinator. Students carried out challenging projects in various Groups of the Centre according to their discipline. During the period of their stay, they visited various facilities at IGCAR, BHAVINI and MAPS. As a part of the curriculum, quiz, project work presentations, group discussions, report writing and viva were done. The valedictory function was held on July 15, 2016 with Dr. Arun Kumar Bhaduri, Director, IGCAR delivering the valedictory address and distributing the certificates to the students.

*Reported by
M. Sai Baba,
Coordinator-BITS Practice School*



Students from BITS Practice School with Dr. S. A. V. Satya Murty, the then Director, IGCAR and senior colleagues of the Centre during the inaugural function

News & Events

Summer Training in Physics & Chemistry (STIPAC-2016)

May 25 - July 3, 2016



Dr. Arun Kumar Bhaduri, Distinguished Scientist and Director, IGCAR and senior colleagues of the Centre with the participants during the valedictory function

Started in 1995, the annual STIPAC programme has evolved over the years to train the pre-final Physics & Chemistry post graduate students across the country both in theoretical and experimental expertise available in IGCAR. The primary objective of this program is to enthuse and encourage students to take up a career in scientific research. The programme generally held during the summer vacation for the students and runs on a theme for every two years. Experts from other institutions are also invited to address and interact with the students.

The 18th edition of this programme coincided with the International year of Light. The theme chosen was "Lasers in Physics & Chemistry". Around one hundred and fifty seven applicants for Physics and eighty applicants for Chemistry were received from which twenty students in each discipline were selected for STIPAC-16, based on their academic credentials quality of their write-up (Physics) and telephonic interview (Chemistry).

The training comprised about hundred hours of lectures on theory and fifty hours of experiments. Class room lectures

were held in forenoons. In the afternoons, the students were encouraged to have a hands on learning experience by either doing project works or carrying out experimental works on various topics. Towards the end of the course, the students gave a presentation on the work done. Further, special lectures were organized in the evenings by inviting professors from premier institutions.

The STIPAC-16 programme was inaugurated by Dr. S. A. V. Satya Murty, the then Director, IGCAR. Dr. A. K. Bhaduri, Director, IGCAR and Dr. P. R. Vasudeva Rao former Director, IGCAR addressed the students on the valedictory day and distributed the certificates to the physics and chemistry students. Dr. P. R. Vasudeva Rao gave a special lecture on "Separations science and nuclear energy: some perspectives".

Site visits to MAPS, BHAVINI and labs at IGCAR were also organized.

*Reported by
Coordinators of STIPAC 2016*

News & Events

Hindi Fortnight Celebration

September 14-28, 2016



A group photo of prize winners with chief guest and organising committee members

Hindi Fortnight was celebrated at IGCAR, Kalpakkam during September 14-28, 2016 with great enthusiasm. As part of this, Hindi Day function was organised on September 2, 2016 at Dr. Rajaramanna Auditorium. Dr. Arun Kumar Bhaduri, Director, IGCAR was the Chief Guest. The programme was presided over by Shri A.K. Vikraman Nair, Director (P & A) who is also the Chairman of Official Language Implementation Committee (OLIC). The Hindi Day messages of Dr. Sekhar Basu, Chairman, AEC & Secretary, DAE and Shri Rajnath Singh, Hon'ble Minister of Home Affairs were read out by Shri Pranay Kumar Sinha and Shri B. K. Nashine, respectively. Dr. Bhaduri and Shri Vikraman Nair addressed the gathering and spoke about the usefulness of Hindi and appealed to spread Hindi in daily activities at the Centre.

Hindi Day function concluded with the vote of thanks by Dr. Awadhesh Mani, Head, LTSS, CMPD.

During the Hindi Fortnight 2016, a variety of Competitions namely, Extempore Speech, Hindi Calligraphy, Essay writing, Hindi Dictation, Noting & Drafting in Hindi, Vocabulary, Poem recitation, GK Quiz and Hindi Song, were conducted for the employees of the Centre which witnessed large participation.

The valedictory function of Hindi Fortnight-2016 was organised on September 28, 2016. Dr. G. Amarendra, Director, MSG & MMG gave away the prizes and consolation prizes to the winners of Hindi competitions.

*Reported by
J. Srinivas, Deputy Director (OL), Administration*

Conference and Meeting Highlights

**10th National Conference
on Recent Advances in Information Technology (READIT-2016)
July 13-14, 2016**



Dr. M. Sai Baba, Convener, READIT & Director, RMG, Dr. Sundeep Oberoi, Global Head, Enterprise Security and Risk Management, TCS, Dr. G. Amarendra, Director, MSG & MMG and Shri E. Soundararajan, SIRD during the release of souvenir at the inaugural function of READIT-2016

The 10th Biennial National Conference on Recent Advances in Information Technology (READIT) was organized by SIRD, IGCAR in association with the Kalpakkam chapter of Madras Library Association (MALA) during July 13-14, 2016 at Sarabhai Auditorium, IGCAR, Kalpakkam, with the theme of 'Information Access in Digital Era'. More than two hundred and sixty delegates including librarians from academic and public domain, Information Technology professionals and research scholars attended the conference.

The conference was inaugurated on July 13, 2016. Dr. M. Sai Baba, Convener, READIT and Director, RMG delivered the welcome address. The ceremony was chaired and presided over by Dr. G. Amarendra, Director, MSG and MMG, IGCAR. In his keynote lecture, he highlighted transition of libraries from static to dynamic and emphasized the need for relevant information access

The chief guest of the conference Dr. Sundeep Oberoi, Global Head, Enterprise Security and Risk Management, Tata Consultancy Services, delivered the keynote address and highlighted the issues in information access in digital era. A souvenir was released by the chief guest. Shri E. Soundararajan, SIRD, Organizing Secretary, READIT proposed the vote of thanks. Dr. Amarendra inaugurated the exhibition of stalls by various vendors representing information science, information technology and library science.

The conference incorporated invited talks by domain experts in information science and technology, oral/poster presentations by research scholars and professionals. Intensive technical discussions on various aspects of Information Sharing, Big data, Cloud computing, Digital content creation, Infrastructure & access methods, Information science in IT and semantic web for knowledge



Dr. Arun Kumar Bhaduri, Distinguished Scientist and Director, IGCAR and colleagues of our Centre with the participants

creation were presented during the conference by reputed persons from INFLIBNET, DRTC, NIT, TCS, IIT, NISCAIR, IT sectors and esteemed universities.

A special technical session was organized for the contributed presentations from research scholars and also a separate poster session for other contributed papers. The conference created a smooth forum and facilitated good interaction among the young researchers, students, professionals and well-known speakers in the area of modern digital technologies.

The conference was concluded on July 14, 2016. During the valedictory gathering, Shri V. Rajendran, SIRD, RMG, IGCAR, delivered the welcome address. Dr. M. Sai Baba presented

the conference summary and highlighted important issues relating to information sharing and access in digital era. Dr. A. K. Bhaduri, Distinguished Scientist & Director, IGCAR delivered the valedictory address. In his valedictory address he highlighted the importance of relevant information access to patrons in helping their research and academic activities. He also shared some of his views on conducting the future READIT. The best paper awards were distributed to the respective authors by Dr. A. K. Bhaduri. Shri E. Soundararajan, thanked one and all, who participated, enlightened and cheered the conference.

*Reported by
M. Sai Baba, Convener, READIT-2016*

Conference and Meeting Highlights

A brief report on Hindi Scientific Seminar August 03, 2016



Dr. G. Amarendra, Director, MSG and MMG inaugurating the seminar

With a view to encourage Scientists/Engineers to submit research papers in official language Hindi, under the auspices of OLIC, IGCAR, Kalpakkam, a one-day Scientific Seminar on the subject "Science and Technology of Nuclear Reactors with Emphasis on Fast Reactors" was held on August 3, 2016 through Hindi medium at Sarabhai Auditorium. About 100 Scientists/Engineers of IGCAR and various other DAE Units located at Kalpakkam viz., BARCF, MAPS, BHAVINI, SRI/AERB participated in this Seminar. In all, 20 research papers were presented in Hindi on various aspects relating of Nuclear Reactors like fuel fabrication, reprocessing, reactor operation and maintenance, quality assurance, project management, safety etc. The seminar

was inaugurated by Dr. G. Amarendra, Director, MSG and MMG, IGCAR and Shri A. K. Vikraman Nair, Director (P&A) presided over the function. Shri B. K. Nashine, Head, DD & RSD and SED welcomed the participants and Dr. Awadhesh Mani, Head, LTSS, CMPD conducted the programme being the convener. Dr. A. K. Tyagi, the then Head, SND and Dr. B. K. Choudhary, Head, DDNS have guided the technical sessions of the seminar. At the end, Shri S. S. Bhoopathy, AO (P) proposed vote of thanks.

*Reported by
J. Srinivas, Deputy Director (OL), Administration*

Conference and Meeting Highlights

Quality Circle Annual Meet (QCAM) - 2016 August 29, 2016



Dr. Arun Kumar Bhaduri and other senior colleagues of the Centre while Shri C. Mani , Former General Manager, BHEL, Trichy delivering the inaugural address

Quality circle is a small group of employees doing similar or related work who meet regularly to identify, analyze and solve work related problems usually led by a senior team member. After completing their analysis, they present their solutions to management for implementation and to improve the performance of the organization. Thus, implemented correctly, quality circles can help the organization to reduce costs, increase productivity and improve employee morale.

In IGCAR, every year Quality Circle Annual Meet (QCAM) is conducted and the QC case studies are presented by the QC teams. QCAM – 2016 was conducted on 29th August 2016 at Convention Centre and SRI Seminar Hall, Anupuram in parallel sessions. Welcome address was delivered by Shri A. Jyothish Kumar, Director, ESG, The Presidential address was delivered by Dr. Arun Kumar Bhaduri, Director, IGCAR. Inaugural Address was delivered by Shri C. Mani, Former General Manager, BHEL, Trichy and vote of thanks by Shri M. Krishnamoorthy, Head, FS, CWD.

Totally twenty three Quality Circles and delegates from all groups (about three hundred members) from IGCAR, schools from Kalpakkam and neighborhood presented

QC case studies in a wide spectrum of topics covering Technical, Research and Development, Services and Education. Professional judges from BHEL Trichy and TVS, Hosur adjudged the QC case study presentations. Under the Mechanical and Manufacturing' stream, the PLUTONIUM QC, CG, bagged 'Dr Placid Rodriguez Memorial Trophy', while EXCEL QC, FRTG bagged the 'Shri M.K. Ramamurthy Memorial Trophy' for Plant Operation and Services category.

During valedictory function, the events were summed up by Shri G. Kempulraj, Head, CWD. The programme was concluded with the valedictory address and the prizes were distributed to the participants by Dr . G. Amarendra, Director, MSG & MMG and Shri G. Srinivasan, Former - Director, ROMG & RDG. Vote of thanks was proposed by Shri T. V. Maran, EIC, ZWS & member secretary, organising committee.

*Reported by
T. V. Maran,
Member Secretary, Apex Steering Committee
on Quality Circles, IGCA, QCAM 2016*

Conference and Meeting Highlights

8th CEA-DAE Steering Committee Meeting on JHR Collaboration September 20, 2016



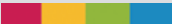
CEA and DAE delegates during the meeting

DAE and CEA have collaborative projects related to material irradiation in Joule Horwitz Reactor (JHR) being built by CEA France at Cadarache. JHR is funded by consortium of few nations in which India is one of the member and France being a lead member. Under this cooperation, many collaborative projects have been taken up. IGCAR is responsible for giving design of sodium loop to be erected in JHR for fast material irradiation testing. Similarly, BARC is responsible for In-Kind support for light water material testing and corrosion loop. 8th CEA-DAE Steering Committee Meeting on JHR Collaboration was held on September 20, 2016 at IGCAR, Kalpakkam for review of ongoing works in IGCAR and BARC. CEA team led by Dr. G. Bignan consisted of four experts where as DAE team consisting of twenty delegates from IGCAR & BARC was led by Dr. A.K. Bhaduri, Director IGCAR. CEA team visited RISHI sodium loop for conducting out of pile test as a prequalification test and witnessed the ongoing experiment. A technical meeting dedicated to review, work related to RISHI loop was also held on September 20, 2016. RISHI loop will be tested in FBTR

and the design will be supplied to CEA for fabrication and erection in JHR. Following ongoing collaborative projects were reviewed during the meeting.

- Development of a sample carrier for testing material at high temperature with online geometrical changes (by BARC)
- Design of a corrosion loop including development of instrumentation for studying Irradiation Assisted Stress Corrosion Cracking (DAE In-Kind contribution) (by BARC)
- Design of smart experiments for getting physical data of fuel sample (by BARC)
- Development of In-Core Sodium Loop for Irradiation of Multiple Samples at JHR (by IGCAR)

*Reported by
B.K. Nashine, Head, SED & DDRSD, FRTG*

 Awards and Honours 

Dr. Rani P. George, Corrosion Science & Technology Division (CSTD), MMG received “Corrosion Awareness Award 2016” for Meritorious Contribution to Research and Education in Corrosion Science & Technology, from NACE International Gateway India Section in 2016.

Dr. Divakar R., Materials Synthesis and Structural Characterisation Division (MSSCD), MMG was conferred Fellowship of the Electron Microscope Society of India during the Annual Meeting of EMSI held during July 2-4, 2016 at IIT BHU, Varanasi.

 Best Paper/Poster Award 

Representing Unstructured Data Using NQSQL: Consistent Hashing Approach using MONGODB

Shri Pabbaraju Chirag Ramdas, Shri E. Soundararajan and Dr. M. Sai Baba

10th National Conference on Recent Advances in Information Technology (READIT-2016)

Indira Gandhi Centre for Atomic Research, July 13-14, 2016

Best Poster Award

Role of Quality Circles in Clean India Mission

Shri S.P. Manivannan

Quality Circle Annual Meet (QCAM) - 2016, Kalpakkam, August 29, 2016

Best Poster Award

Biofouling control of Sea Water Cooled Titanium Condenser Material Through in Situ Application of Alternate Anodic and Cathodic Potential

Shri B. Anandkumar, Dr. Rani P. George, Dr. C. Mallika and Dr. U. Kamachi Mudali

DAE-International Corrosion Conference and Expo (CORCON-2016), New Delhi, September

18 - 21, 2016

Best Poster Award

Estimation of Fatigue Life of Notched Specimens of P91 Steel by Analytical Approaches

Shri J. Veerababu, Shri Sunil Goyal, Dr. R. Sandhya and Dr. K. Laha

2nd International Conference on Fatigue, Durability and Fracture Mechanics (FatigueDurability India

2016), Institute of Structural Integrity and Failure Studies, Indian Institute of Science, Bengaluru,

September 28-30, 2016

Best Paper Award

 **Best Paper/Poster Award** 

Automated Web based System for Task Force/High Level Committees

Ms. M. Kanaga, Ms. J. Jasmine Smila, Ms. Sujatha, Ms. K. Saipriya, Dr. Vidya Sundararajan and Dr. M. Sai Baba

10th National Conference on Recent Advances in Information Technology (READIT-2016)
Indira Gandhi Centre for Atomic Research, July 13-14, 2016

Best Poster Award

Information Management at MRPU: A Case Study

Ms. P. Janupriya, Shri P. P. Muralikannan, Shri Narendra Kumar Kushwaha, Dr. Vidya Sundararajan and Dr. M. Sai Baba

10th National Conference on Recent Advances in Information Technology (READIT-2016)
Indira Gandhi Centre for Atomic Research, July 13-14, 2016

Best Paper Award

Single Window Logon and Federated Gateway for Information Retrieval

Shri Renigunta Vinay Datta, Shri E. Soundararajan and Dr. M. Sai Baba

10th National Conference on Recent Advances in Information Technology (READIT-2016)
Indira Gandhi Centre for Atomic Research, July 13-14, 2016

Best Poster Award

Review of Software Architecture for Data Communication Between Distributed Components of PFBR Full Scope Replica Operator Training Simulator Text Retrieval Models

Shri Jaideep Chakraborty, Ms. Bindu Sankar, Ms. H. Seetha, Shri Nakul Raj Sethi, Ms. T. Jayanthi and Shri K. Madhusoodanan

10th National Conference on Recent Advances in Information Technology (READIT-2016)
Indira Gandhi Centre for Atomic Research, July 13-14, 2016

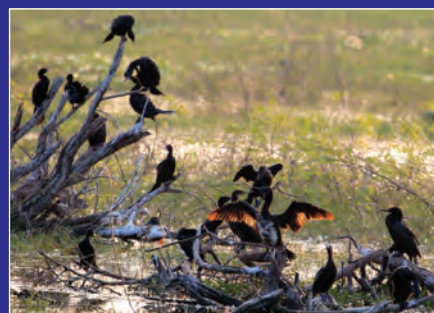
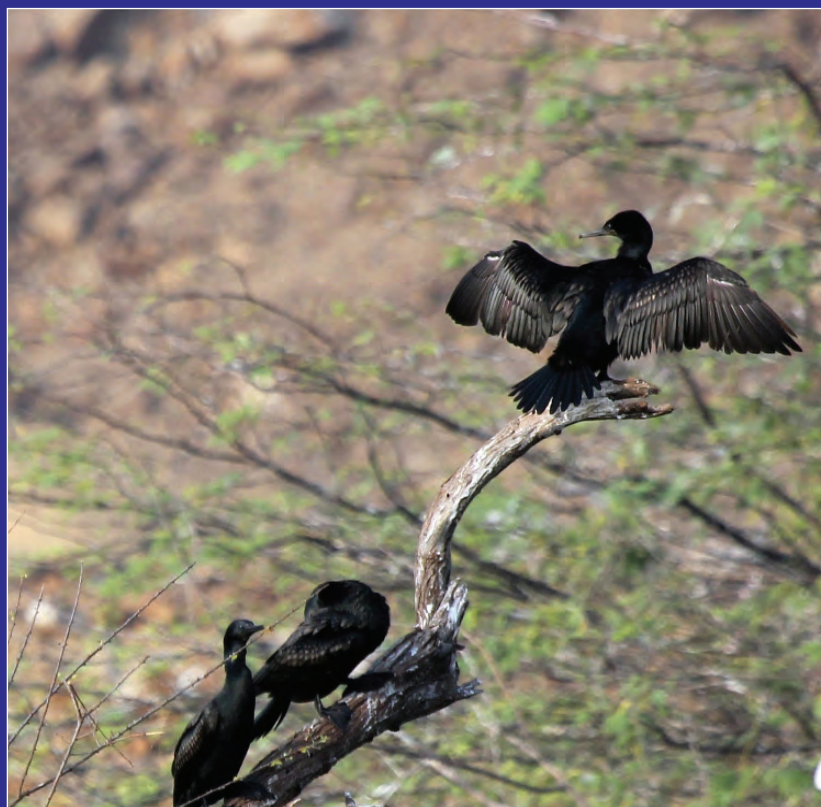
Best Poster Award

Server Consolidation Algorithms using Live Migration of Virtual Machines

Shri Pathikrit Ghosh, Shri E. Soundararajan and Dr. M. Sai Baba

10th National Conference on Recent Advances in Information Technology (READIT-2016)
Indira Gandhi Centre for Atomic Research, July 13-14, 2016

Best Poster Award



Little Cormorant

Dr. M. Sai Baba,

Chairman, Editorial Committee, IGC Newsletter

Editorial Committee Members: Shri M. S. Chandrasekar, Dr. N. V. Chandra Shekar, Dr. T. S. Lakshmi Narasimhan
Dr. C. Mallika, Shri V. Rajendran, Dr. Saroja Saibaba, Dr. C. V. Srinivas and Dr. Vidya Sundararajan